Journal of Materials Chemistry A

Accepted Manuscript

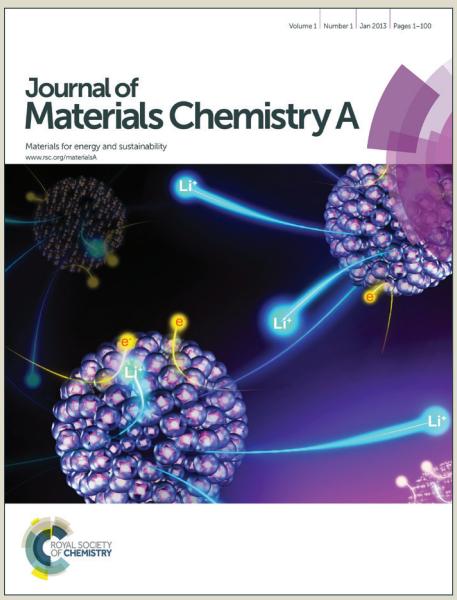

ROYAL SOCIETY OF CHEMISTRY

www.rsc.org/materialsA

Effective adsorption of chromium(VI)/Cr(III) from aqueous solution using ionic liquid functionalized mulitwalled carbon nanotube as a super sorbent

A. Santhana Krishna Kumar[a], Shiuh-Jen Jiang[a,b]*,Wei-Lung Tseng[a,c] *

[a] Department of Chemistry, National Sun Yat-sen University, Kaohsiung 80424, Taiwan.

[b] Department of Medical Laboratory Science and Biotechnology, Kaohsiung Medical University, Kaohsiung 80708, Taiwan.

[c]School of Pharmacy, College of Pharmacy, Kaohsiung Medical University, Kaohsiung 80708, Taiwan. *Corresponding author. Tel: +886-7-5252000 ext. 3929.

E-mail address: sjjiang@mail.nsysu.edu.tw (S.-J. Jiang). +886-7-5252000 ext. 3925

E-mail address: tsengwl@faculty.nsysu.edu.tw (W.-L. Tseng).

Abstract

We report an interesting interaction between multiwalled carbon nanotube (MWCNT's), Tetra n heptylammonium bromide (Ionic Liquid) and total chromium in this studies. IL functionalized MWCNT's which interaction primarily involves electrostatic affinity between the quaternary ammonium cation and surface carboxyl, hydroxyl groups in oxi-MWCNT's. The IL-oxi-MWCNT's adsorbent acts as a host in welcoming the incoming guest hydrochromate anion and several interesting interactions such as cation-π interaction, electrostatic interaction as well as anion-π interaction could be conceptualized in this process. The abundant oxygen-containing functional groups on the surfaces of oxi-MWCNT's plays an important role on Cr(VI)/Cr(III) sorption. Characterization of the adsorbent was performed using various characterization techniques such as cross polarization magic angle spinning nuclear magnetic resonance (^{13}CPMAS-NMR), Raman spectroscopy, x-ray photoelectron spectroscopy(XPS), Powder-x-ray diffraction (Podwer-XRD), Fourier transform infrared spectroscopy (FT-IR), Transmission electron microscope analysis (TEM),

Branauer-Emmett-Teller (BET) isotherm studies, scanning electron microscope (SEM) and energy dispersive x-ray analysis (EDX). The capability of inductively coupled plasma mass spectrometry (ICP-MS) for Cr(VI) adsorption was extensively studied under different optimal parameters and the maximum adsorption capacity was found to be 85.83 mg g^{-1} from nonlinear Langmuir isotherm model. A kinetic study confirms pseudo second order model and the process could be upgraded by column studies to a sample volume of 2000 mL. Effective regeneration of the adsorbent could be accomplished with sodium hydroxide and the potential of this novel adsorbent has been examined in removal of Cr(VI)/Cr(III) from aqueous solutions.

Introduction

Hexavalent chromium Cr(VI) which is highly toxic to living organisms and potentially carcinogenic to humans, is one of the most commonly found pollutants in the environment. Chromium, essentially exists in two forms, namely Cr(VI) and Cr(III).[1] Cr(III) is biologically essential to mammals as it maintains an effective glucose, lipid, and protein metabolism. In contrast, Cr(VI) is highly toxic as it can diffuse as CrO_4^{2-} or $HCrO_4^-$ through cell membranes. The toxicity of Cr(VI) leads to health risks associated with the consumption of Cr(VI) contaminated water.[2] Chromium is generated from various industrial processes, such as electroplating, leather tanning, wood preservations, manufacturing of dye, paint industries, paper industries and petroleum refining processes. The effluents from these industries contain both Cr(VI) and Cr(III) in concentrations ranging from tens to hundreds of milligrams per litre. However, the hexavalent form is 500 times more toxic than the trivalent form and the human toxicity of Cr(VI) ranges from skin irritation to lung cancer, as well as kidney, liver, and gastric damage.[3] Because of these differences, the discharge of Cr(VI) to surface water is regulated to below 0.05 mg L^{-1} by the United States-Environmental Protection Agency (US EPA) while total Cr [including Cr(III) and Cr(VI)] is regulated to below 2 mg L^{-1}. To avoid risk to human health, effective methods must be developed for removing Cr(VI) from water and

wastewater.[4] Among the conventional methods for removing Cr(VI) from water, adsorption methods are preferred because of their efficiency at removing heavy metals such as Cr(VI). In addition, adsorption methods are cost effective compared to other methods.[5] Accordingly, extensive studies have focused on identifying adsorbents that exhibit a high Cr(VI) removal efficiency. Among the validated adsorbents, priority is usually given to adsorption methods because of their environmental and economic advantages. This is especially true for carbon-based adsorbents that are typically the most environmentally friendly and cost effective. Carbon-based adsorbents are considered superior because of for their potential environmental applications, such as the removal of heavy metals with high adsorption capacity and selectivity in aqueous solutions.[6-8]

Carbon nanotubes (CNT's) possess excellent physical and chemical properties and have wide-range potential applications. CNT's small sizes, large surface area, high mechanical strength, and remarkable electrical conductivities indicate their tremendous potential for future engineering applications. CNTs, as defined by Iijima in 1991, have a unique tubular structure with nanometer scale diameters and large length/diameter ratios.[9] CNTs may consist of one (single-walled CNTs, SWCNT's) or up to tens and hundreds (multi-walled CNT's, MWCNT's) of seamless graphene cylinders concentrically stacked with an adjacent layer spacing of approximately 0.34 nm. Owing to the covalent sp^2 bonds formed between individual carbon atoms, CNT's are potentially stiffer and stronger than any other known material.[10] The methods for preparing MWCNTs are simple and MWCNT's can be produced in large scales.[11-15] Owing to their high sorption potential towards heavy metals, both MWCNT's[16] and functionalized MWCNT's have been reported for solid phase extraction of many heavy metal ions from various environmental matrices.[17,18] As a new member of the carbon family, CNT's have exhibited great potential as an attractive adsorbent in wastewater treatment.[19-24] MWCNT's functionalized with various functional groups have proved to be more selective than raw or oxidized MWCNT's because of their exceptional properties for removal of

heavy metals.[25] CNT's functionalized with 2-aminobenzothiazole,[26] iminodiacetic acid,[27] L-cysteine[28] and chitosan,[29] by covalent or non-covalent interactions, have been studied intensively, and the results indicate that MWCNT's are suitable for the heavy metal adsorption from large sample volumes of wastewater treatment.

To the best of our knowledge, IL functionalization onto oxi-MWCNT's for Cr(VI) adsorption has yet to be explored. Here we report that IL- oxi-MWCNT's adsorbent acts as a welcoming host for incoming molecules; hydrochromate anion and several interesting interactions, such as cation-π, electrostatic, and anion-π interactions could be conceptualized in this process. IL functionalization onto oxi-MWCNT's primarily involves electrostatic affinity between the quaternary ammonium cation and surface carboxyl and hydroxyl groups in the oxi-MWCNT's. This IL-oxi-MWCNT's novel adsorbent shows excellent sorption characteristics for Cr(VI)/Cr(III), as substantiated through the comprehensive physico-chemical characterization techniques, batch adsorption study, and column dynamic up gradation to a large sample volume.

Experimental

Preparation of oxidized MWCNT's from MWCNT's

A 1.5g of multi-walled carbon nanotube powder was taken and gradually added to a 9:1 mixture of concentrated H_2SO_4/HNO_3 (180:20 mL). The reaction was slightly exothermic to 40-50 ^{0}C, after which it was heated upto 70 ^{0}C with continuous stirring for 6h. The above reaction mixture was cooled to room temperature. After each wash, the filtrate was centrifuged at 4500 rpm for 30 minutes and the supernatant was decanted off. The left over solid material was dried at room temperature for 24 hours.[30] A 1.5 g of oxi-MCNT's was dispersed in 50 mL of 1.0 Molar Na_2CO_3 solution and the resulting mixture was stirred for 12 hours and then centrifuged several times to isolate the precipitate. The isolated precipitate was washed with Milli-Q water and dried under vacuum.[31]

Preparation of adsorbent

1g of chlorinated oxi-MWCNT's was taken in a round bottom flask followed by slow drop-wise addition of 0.05 molar of Tetra n heptylammonium bromide (IL) which dissolved in acetone medium and was stirred upto 6 hours at room temperature. To remove excess IL, the resulting mixture was washed with acetone several times and dried under vacuum.The un-reacted IL was removed by repeated washing with acetone. The solid was dried at room temperature overnight and used for further adsorption studies. Comprehensive characterization of the adsorbent was done using various physico-chemical techniques to confirm the presence of IL-Oxi-MWCNT's in the adsorbent.[32]

Batch adsorption study

Batch adsorption isotherm studies were carried out with varying concentrations 20 ppm, 50 ppm, 80ppm, 100 ppm, 250ppm and 500ppm of Cr(VI) solution 0.15g of the IL-Oxi-MWCNT's adsorbent were taken for analysis in an aqueous phase volume of 20mL of Cr(VI). At optimum pH (2.5 to 4.0), the amount of Cr(VI) adsorbed (q_e) was obtained by equilibration at various concentrations using the expression q_e:

$$q_e = \frac{(C_o - C_e)\ V}{W} \qquad (1)$$

where C_o and C_e indicate the initial and equilibrium Cr(VI) concentrations respectively, V and W specify the volume of sample solution (L) and the weight (g) of the IL-oxi-MWCNT's adsorbent, respectively. The supernatant was collected for further ICP-MS analysis to determine the Cr(VI) concentration after adsorption (Table T1 supporting information ESI†).[33]

Results and discussion

The powder X-ray diffraction patterns (Fig. 1) of graphite shows a very sharp diffraction peak for graphite at $2\theta = 26.28^0$ (d = 0.33 nm) corresponding to the plane (002), which shifts to 7.70^0 (d = 1.14 nm) on chemical oxidation, indicating the formation of several functional groups. The C-axis spacing increases from 0.33 to 1.14 nm after oxidation from to MWCNT's, due to the creation of the abundant oxygen-containing functional groups on the surfaces of oxi-MWCNT's. MWCNT's gives distinct characteristic peaks observed at 232 nm (corresponding to π-π* transitions of C=C bonds) due to Π electrons of the double bonds in the MWCNT's (Fig. 2) and 302 nm (due to n-π* transitions of COOH groups) a shoulder peak is observed for carboxylated MWCNT's indicating a transition due to an unshared pair of electrons of the -C=O bond in the (-COO) carbonyl group.[34] ^{13}CPMAS-NMR spectroscopy is the most powerful method available to study the detailed chemical structures of carbon-based materials such as MWCNT's. Typical solid state ^{13}CPMAS-NMR spectra revealed that unique isotropic line at 136.4 ppm is well known signature of nanotube. The spectra shows the signal associated with the graphitic sp^2 carbons of the MWCNT's (136.4 ppm), consistent with previous results.[35] In addition to the 112.9 ppm line of the highly purified nanotubes.[36] After oxidation of MWCNT's it shows carbonyl signal at 168.3, which is exceptionally shielded for a carboxylic acid. Thus, the π-system of the nanotube itself appears to exert a significant shielding and broadening effect on the carbonyl carbon of the substituent.[37] The peak at 61.5 ppm is assigned to carbon atoms bonding to the epoxy group and the peak at 136.4 ppm is ascribed to the graphitic sp^2 carbon (Fig. 3). The broad signal from about 140-190 ppm encompasses the range expected for a carboxylic acid (COOH) group.[35] In addition, another three small peaks were also found in high-resolution ^{13}CPMAS-NMR spectrum at about 112.9, 168.3 and 194.4 ppm. These three weak peaks were tentatively assigned to lactol, ester carbonyl and ketone functional groups respectively.[38] The

above observations are in full agreement with the Raman spectroscopic results, Raman spectroscopy is powerful tool to characterize the extent of disorder or degree of crystallinity in the functionalized MWCNT's. The Raman spectrum of MWCNT's shows a D peak at 1343 cm^{-1} (D band) and a very strong peak at 1570 cm^{-1} G band and a 2446 cm^{-1} D' band and 2D band 2674 cm^{-1} (Fig. 4A). After oxidation of MWCNT's shows D band at 1350 cm^{-1} , G bands at 1574 cm^{-1} and 2D band at 2670 cm^{-1} (Fig. 4B). However after oxidation of MWCNT's shows the D and G bands have equal intensity, confirming that MWCNT's completely oxidized and open ends of nanotubes without modifying structure of their sidewalls MWCNT's.[39] The D and G bands at 1343 and 1570 cm^{-1}, respectively, were attributed to the structure of sp^3 and sp^2 hybridized carbon atom,[11,40] indicating that defects/disorder-induced modes and in-plane vibrations of the graphitic wall, can be clearly observed for pure MWCNT's, and after oxidized MWCNT's, respectively. Therefore, the degree of the graphitization of MWCNT's can be quantified by the intensity ratio of D to G bands. The comparable intensity of I_D to I_G indicates the purification of MWCNT's, which is higher intensity of I_D/I_G ratio, is reflective of the higher quality of the carbon nanotubes without defects. The peak intensity ratios (I_D/I_G) were 0.35 and 0.99 for the pure MWCNT's and oxidized MWCNT's samples, respectively. Thus, the largest I_D/I_G ratio of oxidized-MWCNT's sample implies that oxidized-MWCNT's contain more amorphous carbon nature than pure MWCNT's samples.[41] The result implies that harsh chemical acid treatment produces carboxylic acid sites on the surface, causing a significant structural damage of MWCNT's increasing value of I_D/I_G ratio after acid treatment (Fig. 4B) could be attributed to the increase of amorphous carbons and disorder bonds. The above observations are in full agreement with TEM and SEM results, transmission electron microscopy was used to determine possible morphological changes on pure MWCNT's and oxidised MWCNT's. It is clear from the (Fig. 5A&B) that pristine MWCNT's rope-like, curved and highly tangled tubes

with diameters between 100 nm, because of inter-molecular forces, pristine MWCNT's different size and an aggregated structure. As can be seen, a large amount of amorphous carbon appeared in MWCNT's after purification. However, after oxidation with strong oxidants such as nitric acid/sulphuric acid in presence of $KMnO_4$ (Fig. 5C, D &E) some bundles appear exfoliated and curled, especially in the case of strong oxidants treatments, severe fragmentation the average length was estimated to be 200 nm (Fig. 5D). The oxi-MWCNT's structure takes place as clearly indicated, a major alteration of the structural integrity was observed. Thus, the treatment of MWCNT's with strong oxidizing agents causes severe etching of graphitic surface material, leading to tubes shorter length with a large population of disordered sites.[42] The morphologies of MWCNT's were examined (Fig. 6A) nearly uniform monodispersed spheres, after oxidation of MWCNT's surface morphology implying minimal damage during oxidation process. The oxidized MWCNT's shows the clean and smooth surface (Fig. 6B), while the surfaces functionalized MWCNT's with IL reveals that polar surface groups such as carboxyl, hydroxyl and quaternary ammonium cation. Furthermore, the surface morphologies of IL-oxi-MWCNT's appeared to be soft and puffy (Fig. 6C), while functionalized MWCNT's with polar surface groups shows shiny and rigidly sooth morphologies. A dense porous morphology got disturbed after adsorption of Cr(VI) could accommodate onto adsorbent surfaces which observed in the SEM images (Fig. 6D). In addition, energy dispersive spectroscopy (EDX) analysis was utilized to determine the chemical composition, after adsorption of Cr(VI) on to the adsorbent had characteristic peaks (0-1 keV) in the EDX spectrum (Fig. 7) confirms, the presence of adsorbed Cr(VI) along with other elements such as carbon, oxygen, and nitrogen respectively.[43] It's customary to characterize the prepared adsorbent finding out surface area, pore volume, the specific surface area, S_{BET}, was calculated with the Brunauer–Emmett–Teller (BET) equation.[44] The surface areas for the pristine MWCNT's (Fig. S1A of supporting information ESI†) and IL-

oxi-MWCNT's (Fig. S1B of supporting information ESI†) were found to be 62.5 and 87.4 m^2g^{-1}, respectively, which indicated an increase of the surface area functionalized carbon nanotubes compared with the pristine one, due to the good funcationlization of the ionic liquid with oxi-MWCNT's which decreased the tangling and folding of the carbon nanotubes, and as a result, enhanced their accessibility for nitrogen adsorption, these isotherms could be classified as a type IV isotherm, with H3 type hysteresis loops according to the original IUPAC classification.[45,46] The Barrett- Joyner-Halenda (BJH) pore size distribution curve for the adsorbent provides a pore size of 3.7 nm at a maximum pore volume of 0.82 cm^3g^{-1}. However, the prepared adsorbent showed a very good adsorption capacity for Cr(VI) as evident from the relevant adsorption data. This is well corroborated from the supporting evidences such as XPS and EDX spectral analysis which clearly shows the presence of adsorbed Cr(VI) onto the surface of the adsorbent. The FT-IR spectrum (Fig. 8A) shows characteristic peaks for pure MWCNT's corresponding to aromatic C-H stretching at 3416 cm^{-1}, C=C stretching at 1638 &1548 cm^{-1} and C-H bending at 1434 cm^{-1}. After the oxidation with nitric acid/sulfuric acid and $KMnO_4$ functional groups such as hydroxyl, carboxylic acid and epoxy group were introduced. The presence of characteristic bands C=O, O-H, and C-O bonds is due to the formation of COOH groups predominantly on the open end-tips of the nanotubes after oxidation is evident in the IR spectrum shown in Fig. 8B. After oxidation MWCNT's show a broad peak at 3436 cm^{-1} which refers to the O-H stretch of the hydroxyl group which can be ascribed to the oscillation of carboxyl groups. The peak at 3436 cm^{-1} can be assigned to the O-H stretch from carboxyl groups (O=C−OH and C−OH), while the peak at 2450 cm^{-1} can be associated with the O−H stretch from strongly hydrogen-bonded –COOH.[47] The carbonyl group (C=O) stretching vibrations appeared in a new peak at 1740 cm^{-1} whereas the peaks at 1632 & 1370 cm^{-1} can be attributed to the asymmetric and symmetric –

COO− stretching.[35,48] Increased strength of the signal at 1217 cm^{-1} may be associated with C–O stretching in the same functionalities.[47] After funcationalization of ionic liquid the newly formed IL-oxi-MWCNT's bond was slightly downshifted (observed at 1723 cm^{-1}) which is due to coupling with some of the surface functional groups and the Ionic liquid, these spectral shifts could be ascribed to electrostatic interaction of the quaternary ammonium cation with the OH group and the interaction of the π electrons in the polarizable aromatic ring manifested as cation-π interaction (Fig. 8C). In the pH range 2.5-4.0, the hydroxyl groups in the adsorbent (IL–Oxi-MWCNT's) could be protonated and these positively charged surface hydroxyl groups could also interact with the hydrochromate anion ($HCrO_4^-$). After adsorption of Cr(VI) (Fig. 8D) onto the adsorbent two new peaks were appeared at 946 & 723 cm^{-1} characteristic of Cr=O and Cr-O stretching frequencies in the hydrochromate anion.[32] X-ray photoelectron spectroscopy analysis helps in identifying the oxidative state of various elements, the XPS total survey spectrum of IL-oxi-MWCNT's adsorbent is shown in Fig. 9A. The C-1s spectrum (Fig. 9B) was found to peak at the binding energies of 284.8 eV. Whereas the N-1s spectrum (Fig. 9C) was found to peak at the binding energies of 402.2 eV for the tetra n heptyl ammonium cation, which would involve an electrostatic interaction with the surface hydroxyl and carboxyl groups onto the surface of the IL-oxi-MWCNT's. Furthermore, the tetra n heptyl ammonium cation is involved in an ion-pair interaction with the $HCrO_4^-$ anion. The chromium spectra (Fig. 9D) had two major peaks, corresponding to $2p_{3/2}$ and $2p_{1/2}$ core levels of chromium. The BEs for Cr $2p_{3/2}$ are assigned to 577.4 ($CrCl_3$), 577.3 $Cr(OH)_3$, and 576.2 eV (Cr_2O_3) to Cr(III). The Cr $2p_{3/2}$ and Cr $2p_{1/2}$ peaks in the spectrum of the IL-oxi-MWCNT's adsorbent after adsorption of Cr were located at 577.70 and 587.65 eV. These peaks correspond to the oxidation states +3 and +6 respectively. The XPS spectrum of chromium-treated IL-oxi-MWCNT's revealed an extensive reduction of Cr(VI)

sorbed onto trivalent form, indeed these two contributions of the Cr2p peaks of chromium sorbed at 577.70 and 587.65 eV.[49] The XPS data revealed that in acidic medium, Cr(VI) would remain in a dichromate form ($Cr_2O_7^{2-}$), which is a more active and stronger oxidant than the chromate (CrO_4^{2-}) ion. The reduction potentials for dichromate and chromate ions were 1.33 and −0.13 V respectively. With increased contact time, the redox reaction is more favourable on the adsorbent surface due to electron donation from the carboxyl and hydroxyl groups present in oxi-MWCNT. The significant binding energies at 577.70 and 587.65 eV could be attributed to Cr(III), corresponding to the $2p_{3/2}$ and $2p_{1/2}$ orbitals respectively. Therefore, Cr(III) and Cr(VI) were present on the surface of the IL-oxi-MWCNT's adsorbent after adsorption of Cr(VI). This implies that the adsorption process would also involve the reduction of Cr(VI) to Cr(III) on the adsorbent surface.[50,51] The O-1s spectrum (Fig. 9E) shows that the peak corresponding to the binding energy 532.1 eV is attributed to the IL-oxi-MWCNT's adsorbent.

pH Point of Zero Charge (pH_{PZC})

The pH_{pzc} adsorbent surface acquires a neutral charge is referred to as point of zero charge;- pH_{pzc} is one of the key factors that controls the adsorption process on carbon materials; it controls the electrostatic interactions between the adsorbent and the adsorbate. The change of the electrostatic force between Cr(VI) and IL-oxi-MWCNT's explains the pH impact on Cr(VI) adsorption. The pH_{pzc} of the IL-oxi-MWCNT's adsorbent was measured using 25 ^{0}C by taking 0.15 g of adsorbent in 50 mL of 0.1 mol L^{-1} sodium chloride electrolyte solution, the initial pH was adjusted using 0.1 mol L^{-1} HCl or NaOH, with constant magnetic shaking in 150 rpm, after a time period of 24 h, the final pH was measured. The point of zero charge (pH_{pzc}) was determined from the plot of ΔpH [$pH_{initial} - pH_{final}$] versus $pH_{initial}$ (Fig. 10A). The pH_{pzc} was found to be 4.20, it is well known that a solid surface is positively charged at pH< pH_{PZC} and negatively

charged at pH> pH_{PZC}, leading to increased electrostatic attraction or repulsion with anionic Cr(VI) species, thus resulting in more or less ready to adsorption.[52] The pH_{pzc} below this value could be positively charged and favorable for Cr(VI) adsorption. As pH increases, the surface of IL-oxi-MWCNT's becomes less positively charged and the interaction between IL-Oxi-MWCNT's and Cr(VI) becomes less and changes to a repulsive force at pH > 4.20, resulting in significant decrease of Cr(VI) adsorption. Above pH_{pzc}, the surface charge of adsorbent becomes negative with slow deprotonation of the surface hydroxy groups leading to electrostatic repulsion between Cr(VI) oxy anion and the adsorbent surface. This has been well documented in previous literatures of heavy metal adsorption on various adsorbents.[32,53]

Effect of pH and adsorption mechanism

pH is one of the most important parameters controlling the metal ion sorption process. The effect of pH on the removal of Cr(VI) were investigated, adsorption of Cr(VI) by IL-Oxi-MWCNT's was studied by varying the solution pH over a range of 1 to 10 using 0.1 N NaOH/HCl. The functional groups (such as $-COOH$, $-OH_2^+$, $-COO^-$, $-OH$, $-O-$, etc.) on the surfaces of oxidized MWCNT's participate in Cr(VI) adsorption. The pH of the aqueous medium plays an important role in the interaction of hexavalent chromium with IL and oxi-MWCNT's. In aqueous medium, depending on the pH, there exists a well-known equilibrium between the various oxyanions of chromium as given below.[48]

$$H_2CrO_4 \rightleftharpoons H^+ + HCrO_4^- \qquad K_1=1.21$$

$$HCrO_4^- \rightleftharpoons H^+ + CrO_4^{2-} \qquad K_2=3 \times 10^{-7}$$

$$2HCrO_4^- \rightleftharpoons Cr_2O_7^{2-} + H_2O \qquad K_3=35.5$$

According to Pearson's concept hard and soft acids and base (HSAB) principle is classified chromium is categorized as a hard acid and nitrogen is classified as a hard base. It has been well

established that in pH range 2.5 to 4, Cr(VI) exists as $HCrO_4^-$ (hydrogentetraoxochromate anion) and at higher pH the equilibrium favours CrO_4^{2-} (tetraoxochromate) oxyanion. In strongly acidic medium (pH less than 2), the dichromate ion, $Cr_2O_7^{2-}$ predominates in solution.[32] The optimum pH (Fig. 10B) for adsorption of hexavalent chromium onto IL–oxi-MWCNT's adsorbent was observed in the range 2.5 to 4.0. It is quite probable to visualize a cation-π interaction between the quaternary ammonium cation and the aromatic pi-moiety in oxi-MWCNT's. The tetra n heptyl ammonium cation would be involved in an electrostatic interaction with the surface hydroxyl and carboxyl groups onto the adsorbent surface. Furthermore, the quaternary ammonium cation is involved in an ion-pair interaction with the $HCrO_4^-$ anion, as well as with protonated hydroxyl and carboxyl groups, onto the adsorbent surface.[32, 54-56] The overall mechanism that could be conceptualized in this adsorption process is given in Fig. 11. With an increase in pH, the repulsion between the negatively charged oxi-MWCNT's surface (owing to the deprotonation of the surface hydroxyl and carboxyl groups) and the hydrochromate anion results in a decrease in the percentage adsorption. In alkaline pH, the surface charge of the adsorbent becomes negative with the slow deprotonation of the surface hydroxy groups, leading to electrostatic repulsion between the hexavalent chromium oxy anion.[32] At higher pH, Cr(III) exists as $Cr(OH)_2^+$ and $Cr(OH)^{2+}$ species,[32] in alkaline medium, deprotonation of the surface hydroxyl groups, and carboxyl group (O^-, COO^-) acts as an electron donor and facilitates effective electrostatic interaction with the above mentioned positively charged Cr(III) species, thus, Cr(III) is effectively retained at higher pH (Fig. 11C).

Adsorption isotherm studies

A variety of empirical isotherm models were used to review the experimental Cr(VI) adsorption data, these isotherms feature some valuable parameters and the most popular among them are the Langmuir[57] and Freundlich isotherms.[58] The Linear isotherms have been widely employed in

several adsorption studies. However, in the present study, since some of the experimental data points deviate from linearity, the nonlinear model would give a better fit to the data. Accordingly, the Langmuir and Freundlich isotherm data were studied by means of the non-linear model and the relevant plots as well as the isotherm parameters were acquired using the Origin 8.5 software. The various isotherm parameters were given in Table T2 of supporting information (ESI†). The q_{max} obtained from the nonlinear Langmuir model was found to be 85.83 mg g^{-1}. The comprehensive characterization of these isotherms can be obtained through the respective plots and the expressions

$$q_e = \frac{q_m b C_e}{1 + b C_e} \qquad (2)$$

$$q_e = K_F C_e^{1/n} \qquad (3)$$

Although, the coefficient of determination R square has been used in many isotherm studies, the adjusted R square is usually considered to be a better way of expressing the fitting of data since it also takes into account the degrees of freedom involved with the sum of the squares. The coefficient of determination for the above isotherms was close to unity. A still better method to compare the models was obtained through the Akaike's Information Criterion (AIC) statistical methodology [59] The AIC values were obtained through the equations

$$AIC = N\, ln\frac{SSE}{N} + 2N_p + \frac{2N_p(N_p + 1)}{N - N_p - 1} \qquad (4)$$

where N is the number of data points, and N_p refers to the number of parameters in the corresponding models. Furthermore, the AIC values could also be compared using another parameter called as evidence ratio which is defined as

$$Evidence\ Ratio = e^{0.5\Delta_0} \qquad (5)$$

where Δ is the difference in the AIC values between the two models. This comparison method ideally suits several two or three parameter isotherm models. The AIC values for the Langmuir and Freundlich models were shown in Table T2 of supporting information (ESI†), the evidence ratio of 58.34 means that Freundlich model is 58 times more likely to be appropriate than the Langmuir isotherm. This could be ascribed to the fact that, the adsorption would be more random, fast and multilayer adsorption, furthermore, a dimensionless parameter (R_L = 1 / 1 + b C_o) is used to link the energy of adsorption (b) for the Langmuir isotherm in describing the adsorption Cr(VI) onto the IL-Oxi-MWCNT's. The value of R_L for the adsorption of Cr(VI) onto the adsorbent was found to be 0.87 which indicates the applicability of Langmuir isotherm[60,61] in describing the adsorption process. The nonlinear isotherm plots were given in (Fig. S2 of Supporting Information†) and the distinct isotherm parameters given in Table T2 of Supporting Information (ESI†), indicate good affinity of the adsorption Cr(VI) onto the adsorbent. The nonlinear Freundlich isotherm plot (Fig. S2 of Supporting Information†) gives the adsorption intensity (n) in the range 1-10, showing the favourable adsorption of Cr(VI) onto the adsorbent surface.

Adsorption kinetics

About 0.15g of IL-Oxi-MWCNT's adsorbent was added to 20 mL of 20 mg L^{-1} Cr(VI) concentrations was taken for analysis, the initial pH of the solution was adjusted to 2.5-4.0. The Cr(VI) concentrations in solution phase were measured at 5, 10, 20, 25, 30 and 40 mins time intervals with constant agitation 150 Revolutions per minute (RPM). The nonlinear pseudo-first and second order models were used to evaluate the kinetics Cr(VI) adsorption. The non-linearized form of the pseudo-first order equation [62] is generally expressed as

$$q_t = q_e(1 - e^{-K_1 t}) \qquad (6)$$

Where q_e and q_t refers to the adsorption capacity at equilibrium and at time t, respectively, k_1 is the pseudo first order rate constant. The pseudo-second order kinetic model [63-66] is represented as

$$q_t = \frac{k_2 q_e^2}{1 + k_2 q_e t} \qquad (7)$$

Herein, k_2 is the overall rate constant of pseudo-second order adsorption. The kinetic plots were shown in Fig S3 of supporting information (ESI†), the kinetic parameters for these two kinetic models were listed in Table T3 of supporting information (ESI†). The q_e (experimental and calculated) values match well with the second order model. Furthermore, the adjusted R square and the reduced chi square value also illustrate the applicability of the second order model in explaining the adsorption kinetics. The rate of adsorption of Cr(VI) onto the IL-oxi-MWCNT's adsorbent surface could be influenced by

a) external mass transfer where the Cr(VI) is transported from the bulk solution to the external adsorbent surface.

b) intraparticle or pore diffusion, in which the adsorbate Cr(VI) could enter the interior of the adsorbent pore sites.

Amidst these two processes, adsorption is quicker and therefore surface or pore diffusion could influence the adsorption kinetics of Cr(VI). Adsorption step happens relatively fast, the q_e (calculated) and the q_e(experimental) values were in accordance with the second order kinetics these values were found to be 2.58 mgg^{-1} and 2.54 mgg^{-1} respectively.

Adsorption thermodynamics

The thermodynamics study is an important parameter in order to ascertain the feasibility and nature of the adsorption process. The thermodynamic parameters namely, standard free energy (ΔG^0), standard enthalpy (ΔH^0) and standard entropy (ΔS^0) changed and these changes were

determined at various temperature ranges, thermodynamic studies, which gives equilibrium constant, ΔH^0 and ΔS^0 were obtained from the slope and intercept of the van't Hoff plot of lnK against 1/T (Fig. S4A of supporting information ESI†), for an exothermic reaction the slope is positive and the equilibrium constant decreases with increases in temperature.[32]

$$\Delta G^o = -RT\ lnK \qquad (8)$$

$$lnK = \frac{-\Delta H^o}{RT} + \frac{\Delta S^o}{R} \qquad (9)$$

Where is R is the gas constant (J K^{-1} mol^{-1}), T is the temperature in (Kelvin) and K is obtained from the ratio of the concentration of Cr(VI) in the solid and liquid phases respectively. The adsorption of Cr(VI) was more favourable at room temperature and adsorption gradually decreases at higher temperature, these results reveals that the adsorbate–adsorbent interaction weakened at higher temperatures, indicating that higher temperature is not favourable for the adsorption process. The anionic-π, (R-COO^- ---aromatic π moiety), (R-O^- ---aromatic π moiety), cationic- π (R_4N^+---aromatic π moiety) and the electrostatic ($HCrO_4^-$----N^+R_4) interactions are responsible for the compactness[32] and decrease in randomness at the solid-solution interface. The long alkyl chain (hydrophobic tail) orients itself thereby facilitating the head group (R_4N^+) [R= $CH_3(CH_2)_6$] to interact electrostatically with Cr(VI) as mentioned in Fig. 12A. Hence, higher temperature is not favourable for the adsorption process; this indicates that adsorption is favourable at 298 K, the amount of Cr(VI) adsorption decreases with an increase in temperature from 298-333K, lower temperatures are favourable for the adsorption process, which is evident from the ΔG^0 values obtained at different temperatures. The free energy values decreased with rises in temperature,-; negative free energy is a good indication of spontaneous adsorption. The enthalpy change (ΔH^0) was found to be negative indicating the exothermic nature of adsorption (Table T4 of supporting information ESI†). The negative (ΔS^0) shows that there is more

orderliness in the interaction between the IL and oxi-MWCNT's. Hence, the enthalpically beneficial adsorption process coupled with the negative free energy and entropy governs the overall interaction of Cr(VI) with the IL functionalized oxi-MWCNT's.

Amount of adsorbent

In the batch experiments, the amount of the adsorbent varied in the range of (0.025 to 0.20)g, the amount of Cr(VI) adsorbed onto IL-MWCNT's was found to be maximum (99.5 %) in the range of (0.15 to 0.2) g in a 20mL sample volume. The available adsorption sites and the surface area increases by varying the adsorbent amount; therefore, the results reveal an increase in the percentage adsorption of Cr(VI). Although, the percentage adsorption increases with an increase in adsorbent dose, the amount of Cr(VI) adsorbed per unit mass decreases. This fact is supported from the trend in % adsorption which shows a sharp increase initially and later attains its maximum at 0.15 g of the adsorbent (Fig. S4B of supporting information ESI†). The decrease in adsorption capacity with adsorbent dose is attributed to desaturation of adsorption sites in the process of adsorption.

Column studies

Effect of sample volume

On a laboratory scale, a glass column 1.5 cm packing height of adsorbent had chosen for column studies, the column 0.8 cm width, 38 cm length of glass column was packed with 1.5g of IL-oxi-MWCNT's adsorbent. The 1.5 g of the adsorbent was dispersed with 50 mL of Milli-Q water to form slurry and then poured into the column. Cotton was placed at the bottom of the column, at a flow rate of 6 mL min^{-1} adjusted and an optimized pH 2.8, a 2000 mL sample volume of 10 mg L^{-1} Cr(VI) was loaded onto the adsorbent column (Fig. 12B). The supernatant was collected for further ICP-MS analysis to determine the amount of Cr(VI) concentration after adsorption. The percentage adsorption of Cr(VI) at decreased sample volumes above

2000ml,-; the decrease in percentage adsorption could be ascribed to decreased adsorbent-adsorbate interaction. The interactive affinity between Cr(VI) and the positively charged quaternary ammonium cation decreased at higher sample volumes leading to a decrease in the adsorption efficiency. Carbon materials swell when in contact with water and at larger sample volume this phenomena is more prominent. The swelling ability of carbon materials at higher volume would enlarge the adsorbent bed resulting in their decreased affinity towards the metal ion. Onyango et al.,[67] have defined a parameter known as the adsorbent exhaustion rate (AER) as an index for the assessment of the column adsorption efficiency. AER is defined as the ratio of the mass of adsorbent to the sample volume and in the present adsorption system, the adsorbent exhaustion rate was found to be 0.75 g L^{-1}, which is reasonably good for a laboratory column operation. A lower exhaustion rate signifies the effectiveness of the adsorbent column. Hence, it is possible that on an industrial scale, with an increase in the amount of the adsorbent in the column, the upper limit for the sample volume[32] would be enhanced correspondingly.

Adsorbent regeneration

The adsorption capacity and the desorption property are two key parameters to evaluate adsorbent. An ideal adsorbent should not only possess higher adsorption capability, but also show better desorption property, which will significantly reduce the overall cost for the adsorbents. Hence, certain prospective reagents were chosen for desorption of Cr(VI). Ideally, the reagent chosen should be cost effective and not damage the adsorbent bed, some of these reagents have proved their worth in earlier adsorption studies involving Cr(VI).[32] These include reducing agents such as sodium sulfite, sodium metabisulfite, sodium nitrite and L- ascorbic acid as well as reagents such as sodium hydroxide and ammonium hydroxide which could elute Cr(VI) by reducing to the less toxic Cr(III) and also to the corresponding chromate salts (Fig 12C).[32] The order of elution with the above tested reagents were found to be sodium hydroxide

(98.0%) > potassium hydroxide (79.4 %) > sodium sulphite (65.0 %) > ammonium hydroxide (61.0 %) > L-ascorbic acid (39.1%) > sodium nitrite (28.0%) sodium metabi-sulphite (25.3%). Regeneration of the adsorbent was accomplished using NaOH and the potential of this novel adsorbent has been utilized in Cr(VI) detoxification. Regeneration and stability of adsorbent for 3 repetitive cycles is yet another benefit to this interesting adsorbent. We were carried out 6 adsorption-desorption cycles and found that the adsorbent is stable and retained its performance, efficiency for 3 cycles (99.5%). The data pertaining is presented in Fig. S4C of supporting information (ESI†), the adsorbent could be reused for 3 adsorption-desorption cycles without any noticeable decrease in the performance efficiency. Beyond 3 cycles, the available active site in the adsorbent gets saturated, which is not readily available for next adsorption studies due to that the adsorption efficiency decreases gradually. However, after 3 cycles, the percentage adsorption of Cr(VI) decreases, which could be ascribed NaOH leads to a weakening of interaction between Cr(VI) and the adsorbent. This could be attributed to the decrease in the effective interaction between the adsorbent and the adsorbate due to the nonavailability of active sites for adsorption. A 20 mL elution volume from a large initial sample volume of 2000 mL ensures a preconcentration factor of 100 which indicates the efficacy in detoxifying Cr(VI) from aqueous solution.

Effect of foreign ions

Before developing practical applications of this method, it would be useful to establish the effects of certain familiar cations and anions on the adsorption of Cr(VI). To test the effects of diverse ions on performance efficiency, after optimizing the column parameters, we validated the presence of certain major ionic constituents that might interfere with the adsorption of Cr(VI). By this approach, the interference of ions such as Pb^{2+} (100 mg L^{-1}), Cd^{2+} (100 mg L^{-1}), Zn^{2+} (100 mg L^{-1}), Cu^{2+} (100 mg L^{-1}), Co^{2+} (100 mg L^{-1}), Ni^{2+} (100 mg L^{-1}), Fe^{2+} (100 mg L^{-1}),

and Mn^{2+} (100 mg L^{-1}) were examined individually in 100 mL sample volumes containing 10 mg L^{-1} hexavalent chromium (Fig. 13A). The adsorption efficiency of Cr(VI) was not influenced by Cu^{2+}, Cd^{2+}, Co^{2+}, Zn^{2+}, Ni^{2+}, or Pb^{2+} , while Fe^{2+} and Mn^{2+} did interfere by reducing the hexavalent chromium to a trivalent state.[32] In addition, ferrous and manganese also known to reduce Cr(VI) to the trivalent state, cationic species interfere by competing for the active binding sites in the adsorbent. In the case of anionic species (i.e., at 100 mg L^{-1} levels of nitrite, chloride, sulphite, and phosphate, adsorption of Cr(VI) was inhibited by competition for the $HCrO_4^-$ ion at the active sites of the IL-oxi-MWCNT's adsorbent (Fig. 13B). Under the given experimental conditions, these ions did not form stable ion-pairs with the quaternary ammonium cation and thus did not compete with the bichromate for the active sites in the adsorbent. However, at higher concentrations (i.e., >250 mg L^{-1}) the sulphite and nitrite anions interfered by reducing the hexavalent chromium to the trivalent state. However, in the presence of excess chloride, it is possible that Ni^{2+}, Cd^{2+}, Co^{2+}, Pb^{2+}, Mn^{2+} and Zn^{2+} could form tetrahalo complexes, which would compete with $HCrO_4^-$ for adsorption and result in a decrease in selectivity.[32]

Comparison of adsorption capacity with literature data

The IL-functionalised oxi-MWCNT's adsorbent was compared in terms of adsorption capacity with some recently reported adsorbents. From the results (Table 1) it is evident that the adsorption capacity of the proposed adsorbent compares favourably with other adsorbents and its adsorption capacity are quite high compared to other adsorbents. [68-71]

Conclusions

In summary, we have demonstrated IL -oxi-MWCNT's adsorbent has shown admirable ability towards the adsorption of Cr(VI) has been illustrated in this work. The tetra n heptyl ammonium cation(IL) was involved in an electrostatic interaction with the surface of hydroxyl and carboxyl

groups onto the adsorbent. Furthermore, quaternary ammonium cation is involved an ion-pair interaction, with the $HCrO_4^-$ anion as well as protonated hydroxyl groups, carboxyl group onto the adsorbent surface. The adsorption of Cr(VI) correlated with the Freundlich isotherm, maximum adsorption capacity found to be 85.83 mg g^{-1}, and Cr(VI) adsorption processes reached their equilibrium state within 40 mins, which is faster than most other carbon -based adsorbents. The method could be scaled up to a large sample volume, as low as 1 ppm of Cr(VI) could be effectively adsorbed in the column. Regeneration of the adsorbent was accomplished using NaOH and the potential of this novel adsorbent has been utilized in Cr(VI) detoxification. Regeneration and stability of adsorbent for 3 repetitive cycles is yet another benefit to this interesting adsorbent; there is considerable change in the adsorption of Cr(VI) from aqueous phase in the presence of various cations and anions. The IL -functionalized oxi-MWCNT's adsorbent has carved a niche among the various other carbon-based adsorbents for adsorption of Cr(VI)/Cr(III).

Acknowledgments

The authors greatly acknowledge financial support of the Taiwan National Science Council under grant NSC: 100-2113-M-110-002-MY3. We also thank Ministry of Science and Technology (MOST) of Republic of China MOST-102-2811-M 110-039 for the post-doctoral grant.

References

(1) B. Qiu, H. Gu, X. Yan, J. Guo, Y. Wang, D. Sun, Q. Wang, M. Khan, X. Zhang, B. L. Weeks, D. P. Young, Z. Guo and S. Wei, *J. Mater. Chem. A,* 2014, **2,** 17454–17462.

(2)B. Qiu, C. Xu, D. Sun, H. Wei, X. Zhang, J. Guo, Q. Wang,D. Rutman, Z. Guo and S. Wei, *RSC Adv.,* 2014, **4,** 29855–29865.

(3)V. K. Gupta, A. Rastogi and A. Nayak, *J. Colloid Interface Sci.*, 2010, **342,** 135 – 141.

(4)A. Baral and R.D. Engelken, *Environ. Sci. Policy*., 2002, **5,** 121–133.

(5)A. Dabrowski, *Adv. Colloid Interface Sci.*, 2001, **93,** 135 – 224.

(6) W. C. Song, J. Hu, Y. Zhao, D. Shao and J. Li, *RSC Adv.,* 2013, **3,** 9514- 9521.

(7) J. T Zhang, Z. Y. Jin, W. C. Li, W. Dong and A. H. Lu, *J. Mater. Chem. A,* 2013, **1,** 13139–13145.

(8)X. Yang, C. G. Chen, J. Li, G. Zhao, X. Ren and X. Wang, *RSC Adv.,* 2012, **2,** 8821–8826.

(9)S. Iijima, *Nature*, 1991, **354,** 56–58.

(10) P. X. Hou, C. Liu and H.M. Cheng, *Carbon,* 2008, **46,** 2003-2025.

(11)A. B. Dichiara, T. J. Sherwood and R. E. Rogers, *J. Mater. Chem. A,* 2013, **1,** 14480–14483.

(12)Y. Liao, Q. Li, Y. Yue and S. Shao, *RSC Adv.,* 2015, **5,** 3232–3238.

(13)A. B. Dichiara, T. J. Sherwood, J. Benton-Smith, J. C. Wilson, S. J. Weinstein and R. E. Rogers, *Nanoscale,* 2014, **6,** 6322–6327.

(14)A. B. Dichiara, J.Benton-Smith and R. E. Rogers, *Environ. Sci.: Nano.,* 2014, **1,** 113–116.

(15)A. B. Dichiara, J. Yuan, S.Yao, A. Sylvestre, L. Zimmer and J. Bai, *J. Mater. Chem. A,* 2014, **2,** 7980–7987.

(16) M. Zhang, B. Gao, X. Cao and L.Y. Yang, *RSC Adv.*, 2013, **3,** 21099–21105.

(17)S.Yang, D. Shao, X. Wang and M. Nagatsu, *RSC Adv.,* 2014, **4,** 4856–4863.

(18)Z.Tian, B. Yang, G. Cui, L. Zhang, Y. Guo and S.Yan, *RSC Adv.,* 2015, **5,** 2266–2275.

(19)Y. Liao, Q. Li, Y.Yue and S. Shao, *RSC Adv.,* 2015, **5,** 3232–3238.

(20)L. H. Zhang, Q. Sun, D.H. Liu and A. H. Lu, *J. Mater. Chem. A.,* 2013, **1,** 9477–9483.

(21) C. Lu, H. Ciu and C. Liu, *Ind. Eng. Chem. Res.,* 2006, **45,** 2850-2855.

(22)M. Kandah and J. L. Meunier, *J. Hazard. Mater.,* 2007, **146,** 283 – 288.

(23)X. K. Wang, C. L. Chen, W. P. Hu, A. P. Ding, D. Xu and X. Zhou, *Environ. Sci. Technol.,* 2005, **39,** 2856 – 2860.

(24)A. Stafiej and K. Pyrzynska, *Sep. Purif. Technol.,* 2008, **58,** 49 – 52.

(25)Z. P. Zang, Z. Hu, Z.H. Li, Q. He and X.J. Chang, *J. Hazard. Mater.*, 2009, **172,** 958 – 963.

(26) R. J. Li, X. J. Chang, Z. H. Li, Z.P. Zang, Z. Hu, D.D. Li and Z.F. Tu, *Microchim. Acta*, 2011, **172,** 269 – 276.

(27) J. P. Wang, X.X. Ma, G. Z. Fang, M. F. Pan, X. K.Ye and S.Wang, *J. Hazard. Mater.,* 2011, **186,** 1985-1992.

(28)Y. Liu, Y. Li and X.P.Yan, *Adv. Funct. Mater.,* 2008, **18,** 1536 – 1543.

(29)Z.G. Wu, W. Feng, Y.Y. Feng, Q. Liu, X. H. Xu, A. Fujii and M. Ozaki, *Carbon,* 2007, **45,** 1212-1218.

(30) B. Dai, M. Cao, G. Fang, B. Liu, X. Dong, M. Pan and S.Wang, *J. Hazard. Mater.*, 2012, **219–220,** 103– 110.

(31) J. Balapanuru, J.X. Yang, S. Xiao, Q. Bao, M. Jahan, L. Polavarapu, J. Wei, Q.H. Xu and K. P. Loh, *Angew. Chem. Int. Ed.,* 2010, **49,** 6549 –6553.

(32)A. Santhana Krishna Kumar and N. Rajesh, *RSC Adv.,* 2013, **3,** 2697-2709.

(33) L. Zhang, W. Xia, X. Liu and W. Zhang, *J. Mater. Chem. A,* 2015, **3,** 331–340.

(34)H. Hu, B. Zhao, M.A. Hamon, K. Kamaras, M. E. Itkis and R. C. Haddon, *J. Am. Chem. Soc.,* 2003, **125,** 14893-14900.

(35)L. Zeng, L. B. Alemany, L. C. Edwards and A. R. Barron, *Nano Res.,* 2008, **1,** 72- 88.

(36) C. G. Bac, P. Bernier, S. Latil, V. Jourdain, A. Rubio, S. H. Jhang, S. W. Lee, Y. W. Park, M. Holzinger and A. Hirsch, *Curr. Appl. Phys.,* 2001, **1,** 149-155.

(37) H. Peng, L. B. Alemany, J. L. Margrave and V.N. Khabashesku, *J. Am. Chem. Soc.,* 2003, **125,** 15174- 15182.

(38) W. Gao, M. Majumder, L.B. Alemany, T.N. Narayanan, M. A. Ibarra, B. K. Pradhan and P.M. Ajayan, *ACS Appl. Mater. Interfaces*, 2011, **3,** 1821–1826.

(39) I. D. Rosca, F. Watari, M. Uo and T. Akasaka, *Carbon,* 2005, **43,** 3124–3131.

(40) Y. Zhao, X. Yang, L. Zhan, S. Ou and J. Tian, *J. Mater. Chem.,* 2011, **21,** 4257–4263.

(41) Y. Zhao, X. Yang and J. Tian, *Electrochim. Acta,* 2009, **54,** 7114-7120.

(42) Y. Wang, X. Song, S. Shao, H. Zhong and F. Lin, *RSC Adv.,* 2012, **2,** 7693-7698.

(43)M. A. Atieh. *Procedia Environ. Sci.,* 2011, **4,** 281–293.

(44) B. Brunauer, P. H. Emmett and E. Teller, *J. Am. Chem. Soc.*, 1938, **60,** 309-319.

(45) K.S.W. Sing, D.H. Everett, R.A.W. Haul, L. Moscou, R. A. Pierotti, J. Rouquerol and T. Siemieniewska, *Pure Appl. Chem.,* 1985, **57,** 603–619.

(46)S. A. Kosa, G. Al-Zhrani and M. Abdel Salam, *Chem. Eng. J.*, 2012, **181– 182,** 159– 168.

(47) G. Ovejero, J. L. Sotelo, M. D. Romero, A. Rodrıguez, M. A. Ocana, G. Rodriguez and J. Garcia, *Ind. Eng. Chem. Res.,* 2006, **45,** 2206–2212.

(48) N. Sankararamakrishnan, M. Jaiswal and N. Verma, *Chem. Eng. J.,* 2014, **235,** 1 – 9.

(49) J. Hu, C. Chen, X.X. Zhu and X. Wang. *J. Hazard. Mater.,* 2009, **162,** 1542 – 1550.

(50) D. Park, Y.S. Yun and J.M. Park, *J. Colloid Interface Sci.,* 2008, **317,** 54–61.

(51) D. Dinda, A. Gupta and S. K.Saha, *J. Mater. Chem. A,* 2013, **1,** 11221–11228.

(52) G. Sheng, Y. Li, X. Yang, X. Ren, S. Yang, J. Hu and X. Wang, *RSC Adv.,* 2012, **2,** 12400–12407

(53) M. Barathi, A. S. K. Kumar, C. Uday kumar and N. Rajesh, *RSC adv.,* 2014, **4,** 53711-53721.

(54) J. Zhu, H. Gu, J. Guo, M. Chen, H. Wei, Z. Luo, H. A. Colorado, N. Yerra, D. Ding, T. C. Ho, N. Haldolaarachchig, J. Hopper, D. P. Young, Z. Guo and S. Wei, *J. Mater. Chem. A,* 2014, **2,** 2256–2265.

(55) Y. L. F. Musico, C. M. Santos, M. L. P. Dalida and D. F. Rodrigues, *J. Mater. Chem. A,* 2013, **1,** 3789–3796.

(56) X.Liu, Y. Gao, H. Luo and R. Jin, *RSC Adv.,* 2014, **4,** 9594–9601.

(57) I. Langmuir, *J. Am. Chem. Soc.,* 1918, **40,** 1361–1403.

(58) H. M. F. Freundlich, *Z. Phys. Chem.,* 1906, **57,** 385-470.

(59) M.I. El-Khaiary and G.F. Malash*, Hydrometallurgy* 2011, **105,** 314–320.

(60) K. R. Hall, L. C. Eagleton, A. Acrivos and T. Ver Meulen, *Ind. Eng. Chem. Fundam.*, 1966, **5,** 212−218.

(61) K. V. Kumar*,* K. Porkodi and F. Rocha, *J. Hazard. Mater.*, 2008, **150,** 158–165.

(62) S. Lagergren, *K. Sven Vetenskapsakad Handl.,* 1898, **24,** 1-39.

(63) Y. S. Ho, *J. Hazard. Mater.*, 2006, **136,** 681–689.

(64) S. Chowdhury and P. Das saha, *Bioremediation J*, 2011, **15,** 181–188.

(65) S. Chowdhury and P. Saha, *Bioremediation J*, 2010, **14,** 196–207.

(66) S. Chowdhury and P. Saha, *Desalin. Water Treat.,* 2011, **30,** 229–236.

(67) M. S. Onyango, T. Y. Leswifi, A. Ochieng, D. Kuchar, F. O. Otieno and H. Matsuda, *Ind. Eng. Chem. Res.* 2009, **48,** 931−937.

(68)G. Gollavelli, C. C. Chang and Y. C. Ling, *ACS Sustainable Chem. Eng.*, 2013, **1,** 462−472.

(69)Y. Wu, H. Luo, H. Wang, C. Wang, J. Zhang and Z. Zhang, *J. Colloid Interface Sci.,* 2013, **394,** 183–191.

(70)M. Liu, T. Wen, X. Wu, C. Chen, J. Hu, J. Li and X. Wang, *Dalton Trans.,* 2013, **42,** 14710–14717.

(71)C. Jung, J. Heo, J. Han, N. Her, S. J. Lee, J. Oh, J. Ryu and Y. Yoon, *Sep. Purif. Technol.,* 2013, **106,** 63-71.

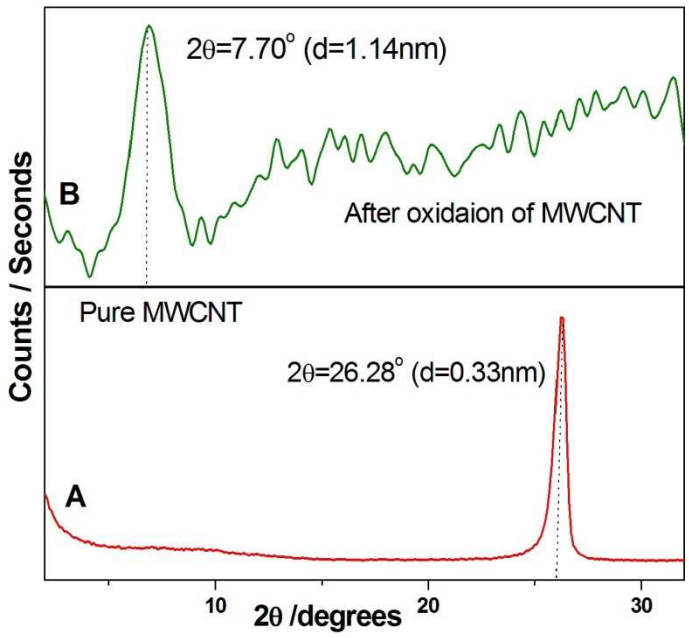

Fig. 1. Powder XRD pattern of (A) pure MWCNT's (B) oxidized –MWCNT's.

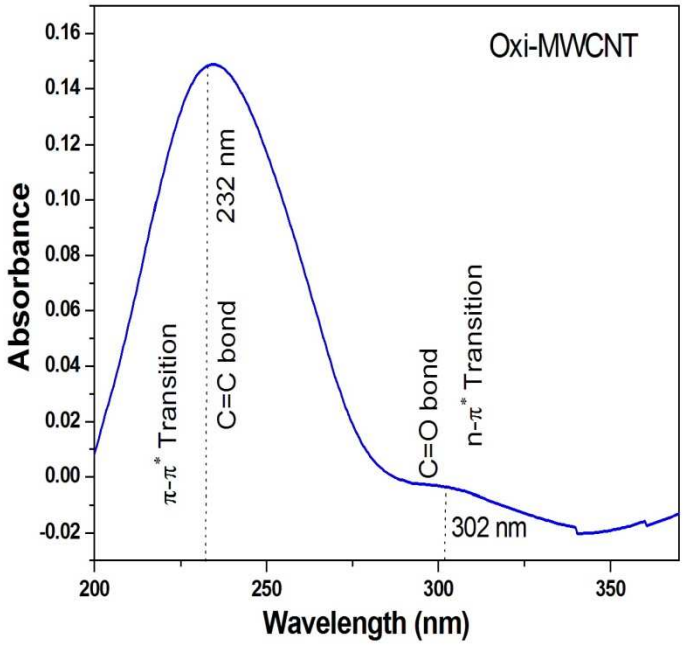

Fig. 2. UV spectrum of oxidized –MWCNT's.

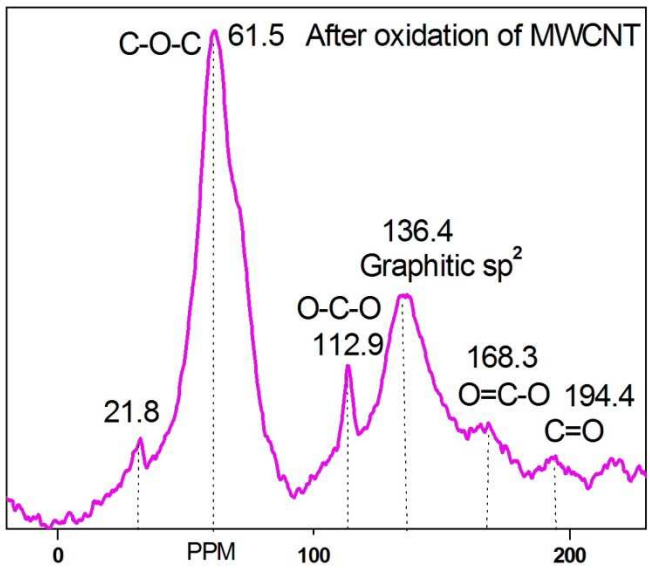

Fig. 3. Solid-state ^{13}C magic-angle spinning (MAS) NMR spectra of oxidized MWCNT's.

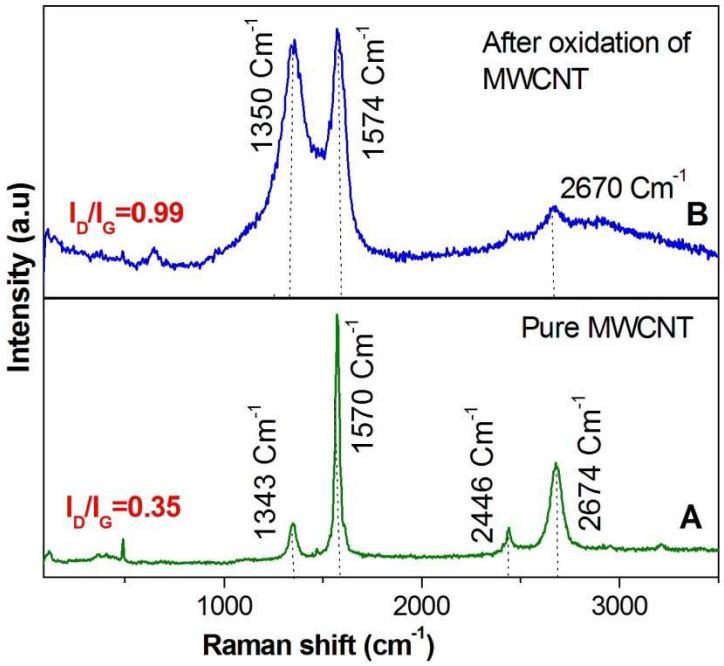

Fig. 4. Raman spectrum of (A) pure MWCNT's (B) oxidized –MWCNT's.

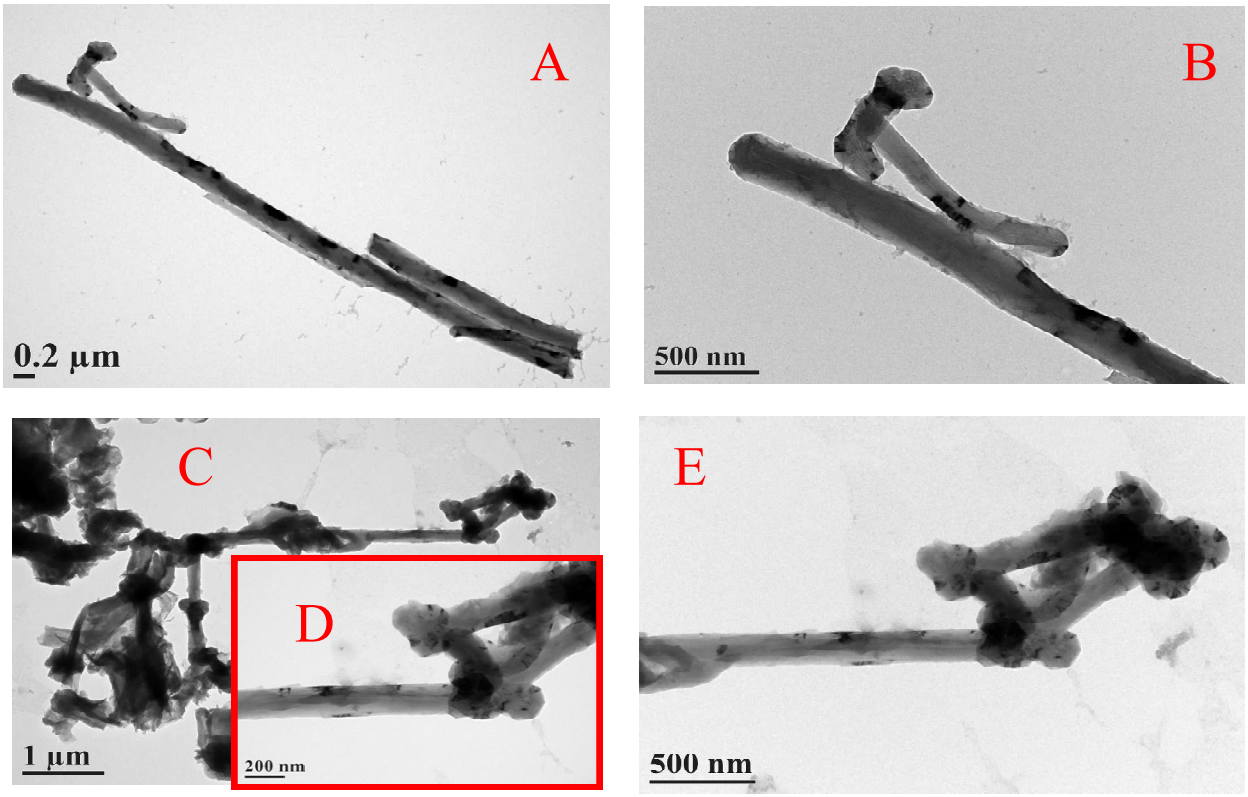

Fig. 5. TEM images of (A) Pure MWCNT's overview (B) Pure MWCNT's (C) oxidised-MWCNT's overview (E) oxidised-MWCNT's.

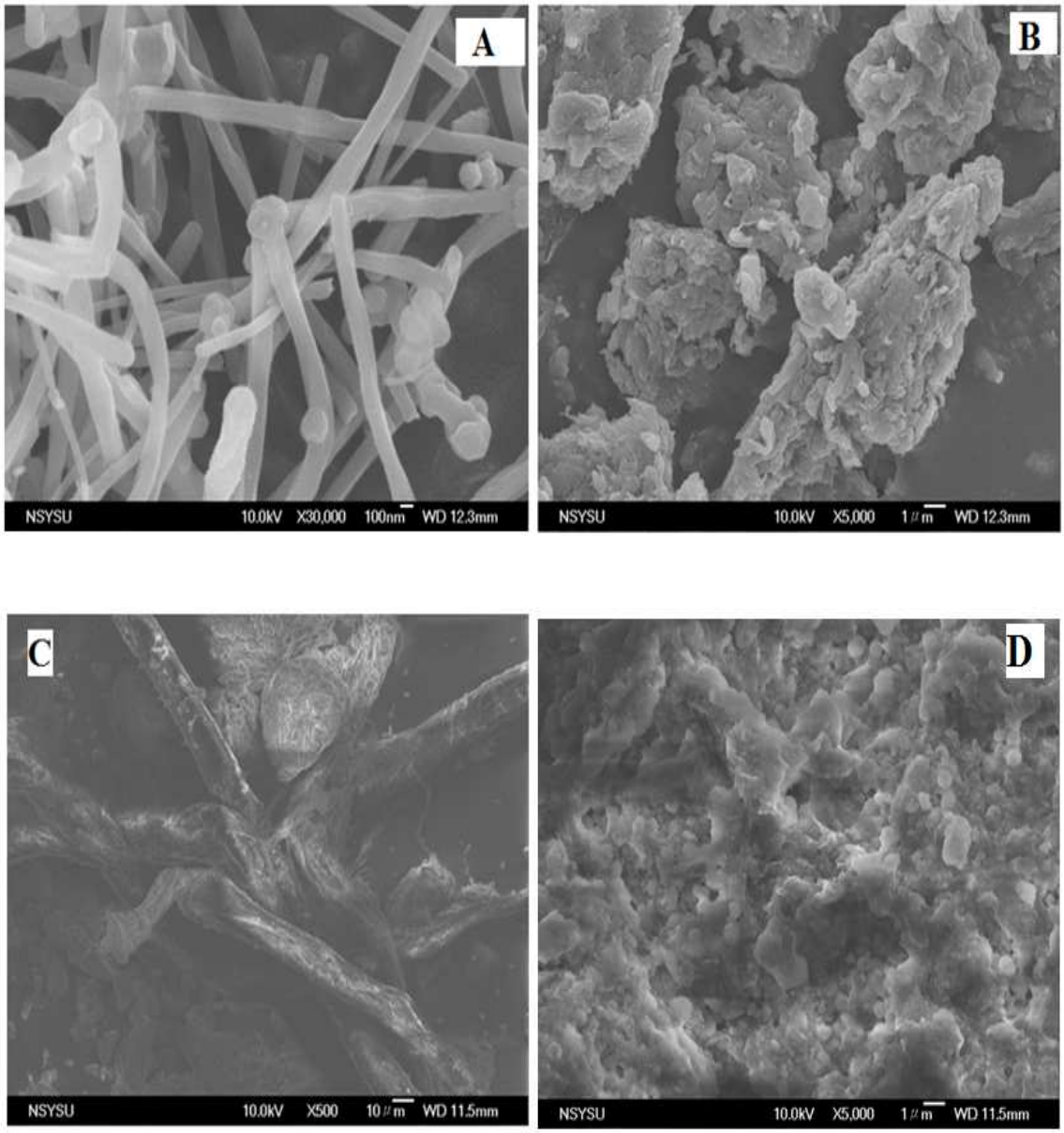

Fig. 6. SEM images of (A) pure MWCNT's (B) oxidized –MWCNT's
(C) IL- functionalized- oxi-MWCNT's
(D) after adsorption of Cr(VI) onto IL-oxi-MWCNT's

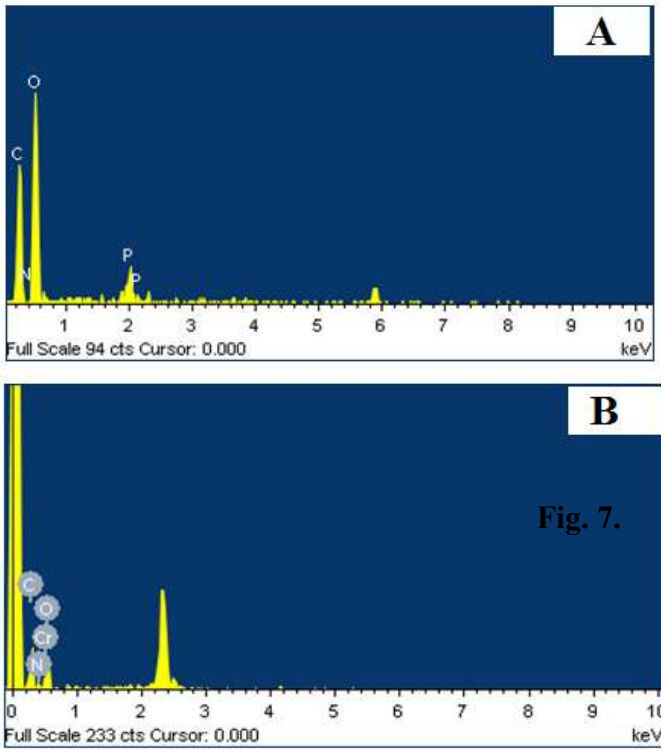

Element	Weight%	Atomic%
C K	35.80	43.63
N K	1.72	1.80
O K	56.64	51.82
P K	5.84	2.76
Totals	100.00	

Element	Weight%	Atomic%
C K	30.29	47.76
N K	12.86	17.39
O K	17.27	20.44
Cr L	39.58	14.41
Total	100.0	

Fig. 7.

Fig. 7. EDX spectrum of (A) IL- functionalized- oxi-MWCNT's

(B) after adsorption of Cr(VI) onto the adsorbent.

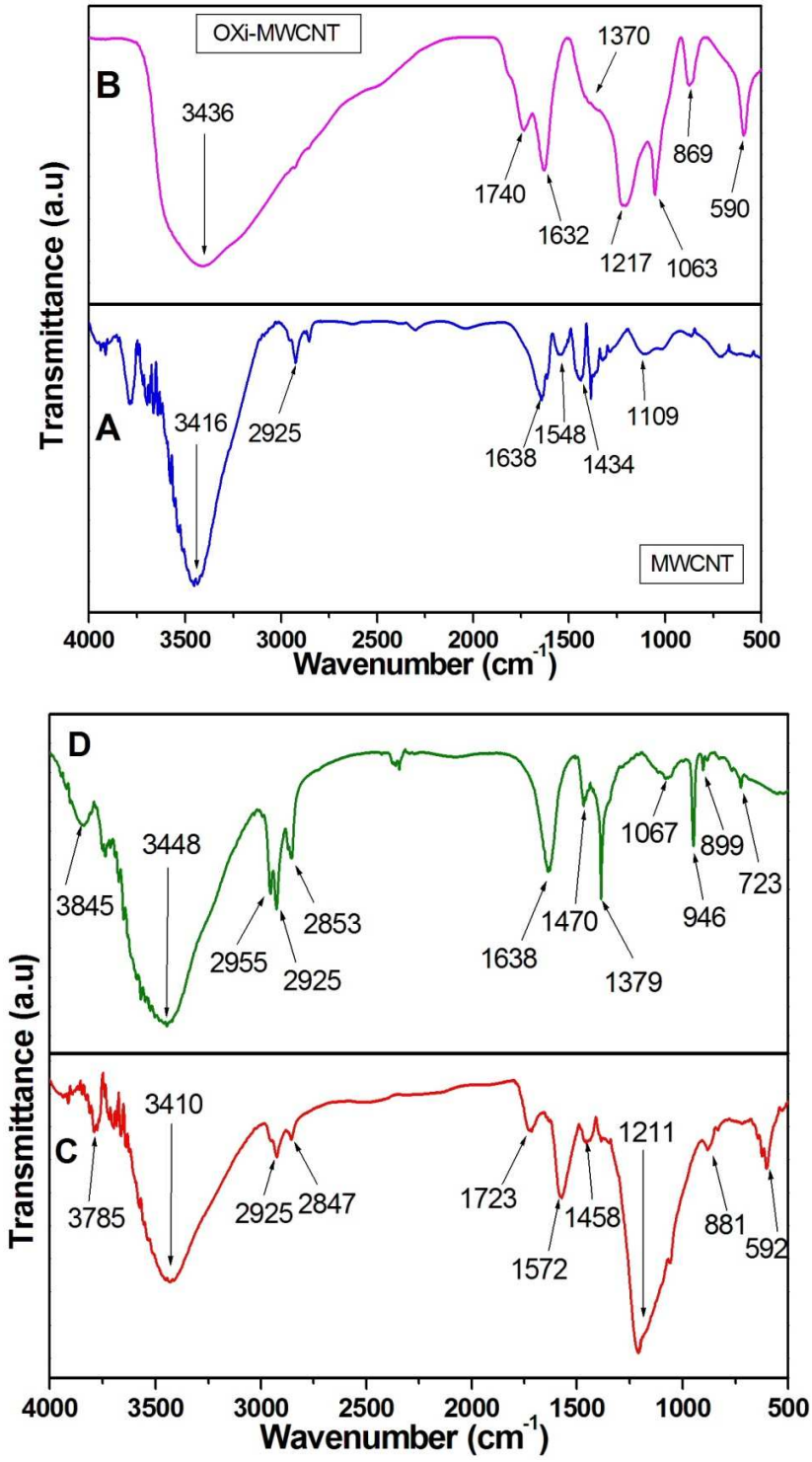

Fig. 8. FT-IR spectrum of (A) pure MWCNT's (B) oxidized –MWCNT's
(C) IL- functionalized oxi-MWCNT's
(D) after adsorption of Cr(VI) onto adsorbent.

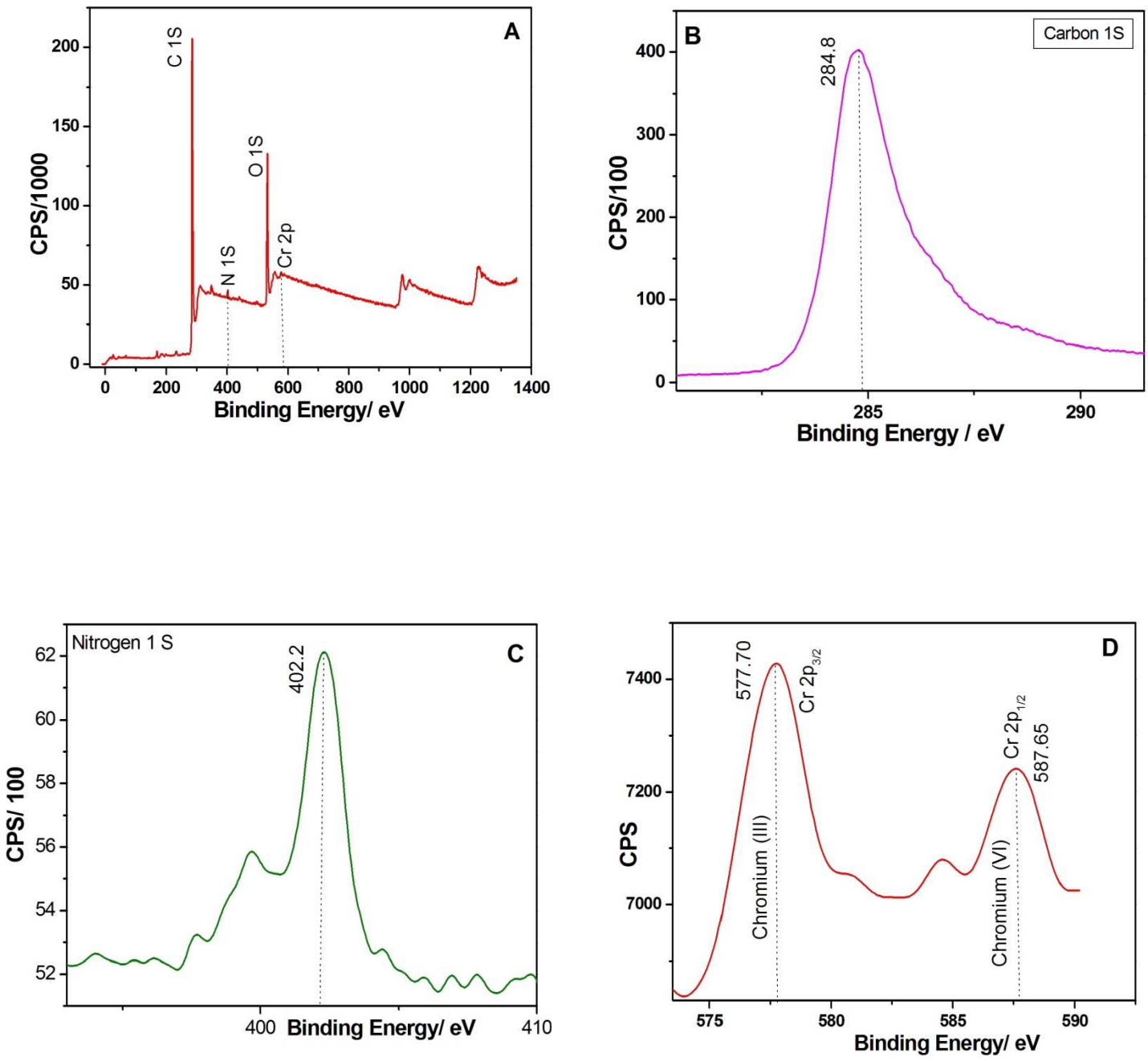

Fig. 9. X-ray photoelectron spectroscopy of after Cr(VI) adsorption onto the adsorbent (A) total survey scan of XPS spectra (B) carbon 1s spectrum of after Cr(VI) adsorption (C) nitrogen1s spectrum of after Cr(VI) adsorption (D) after adsorption of chromium spectrum.

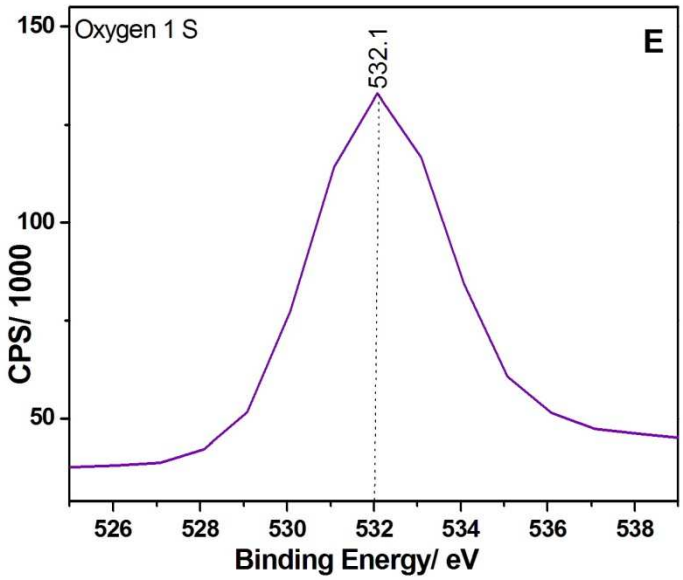

Fig. 9E Oxygen 1s spectrum of after Cr(VI) adsorption.

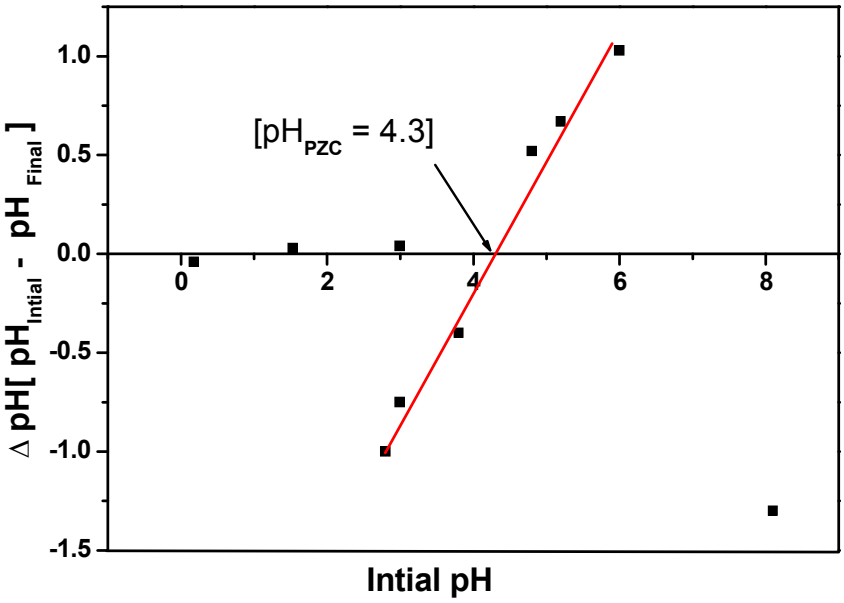

Fig. 10A pH Point of Zero Charge (pH_{PZC}).

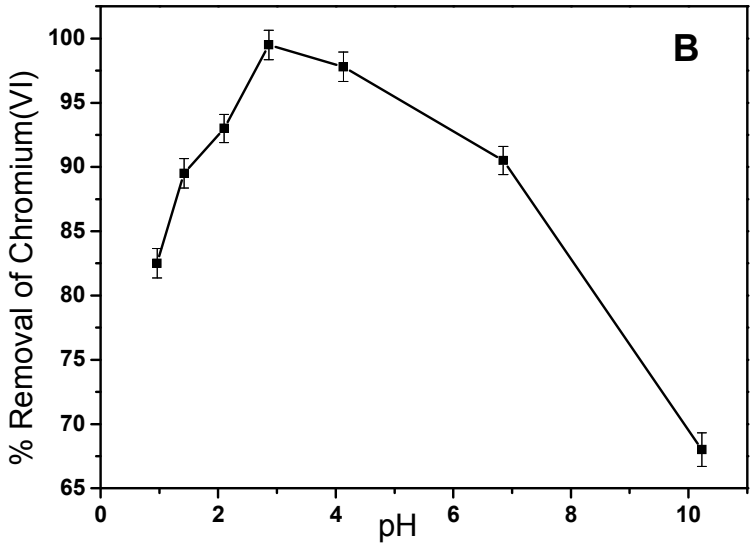

Fig. 10B Effect of pH

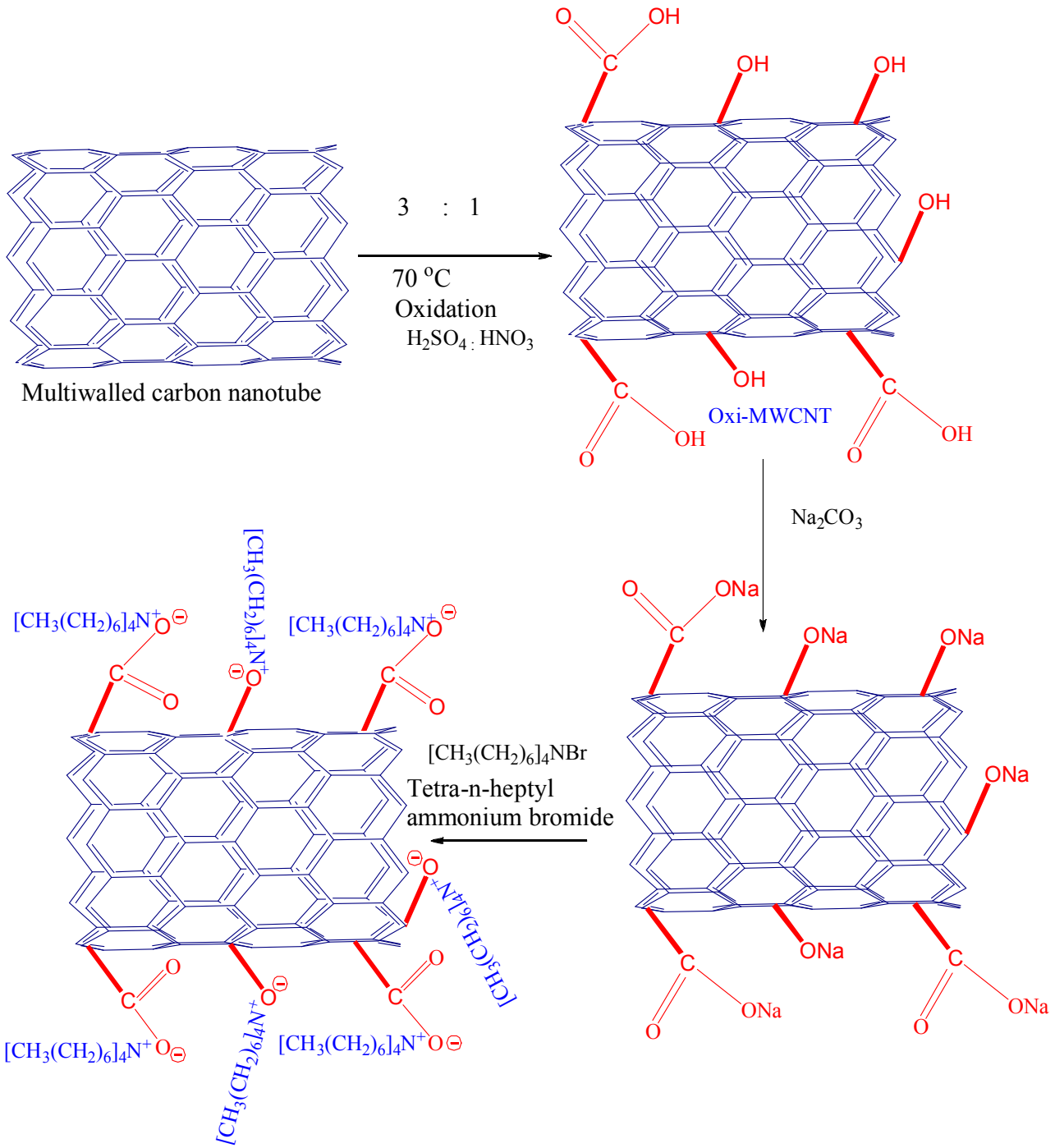

Fig11A. Illustration of interaction between IL and oxi-MWCNT's.

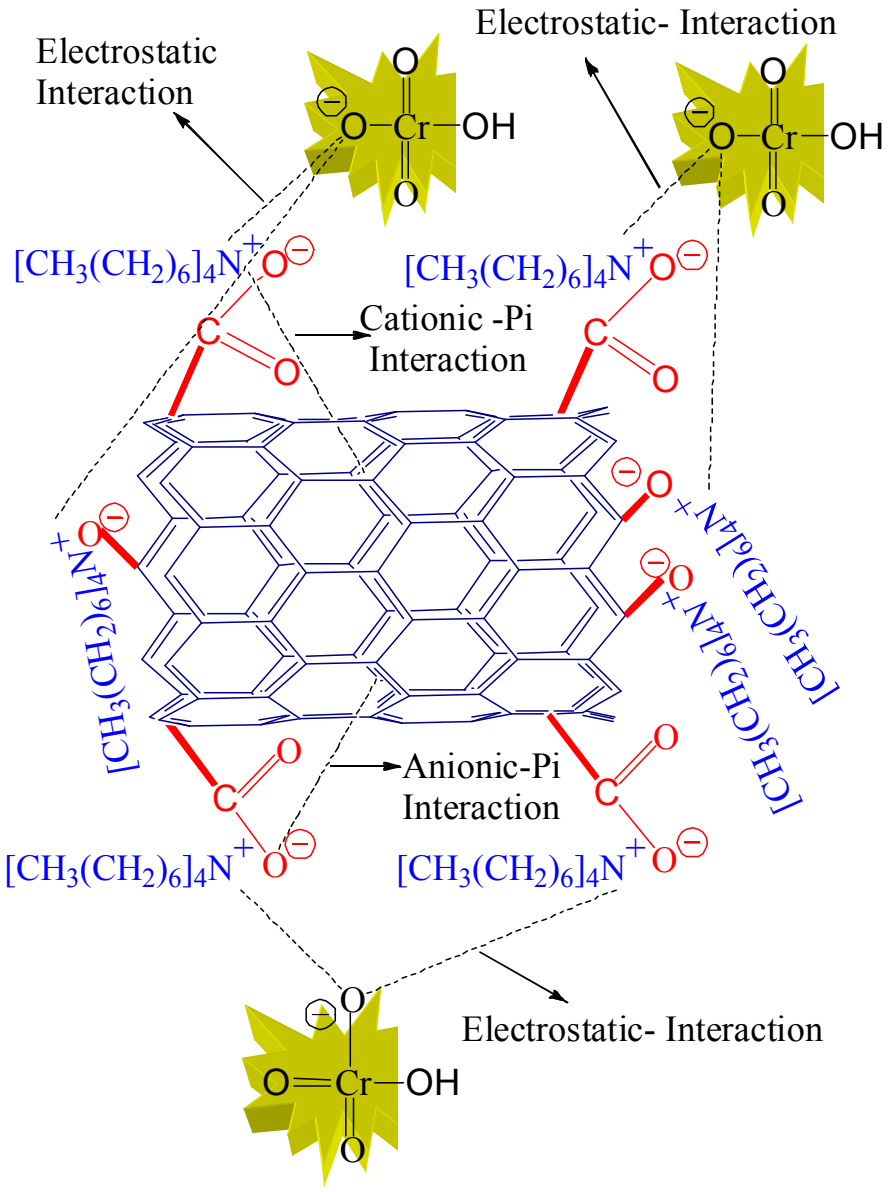

Fig. 11B. Illustration of interaction between IL-oxi-MWCNT's and Cr(VI).

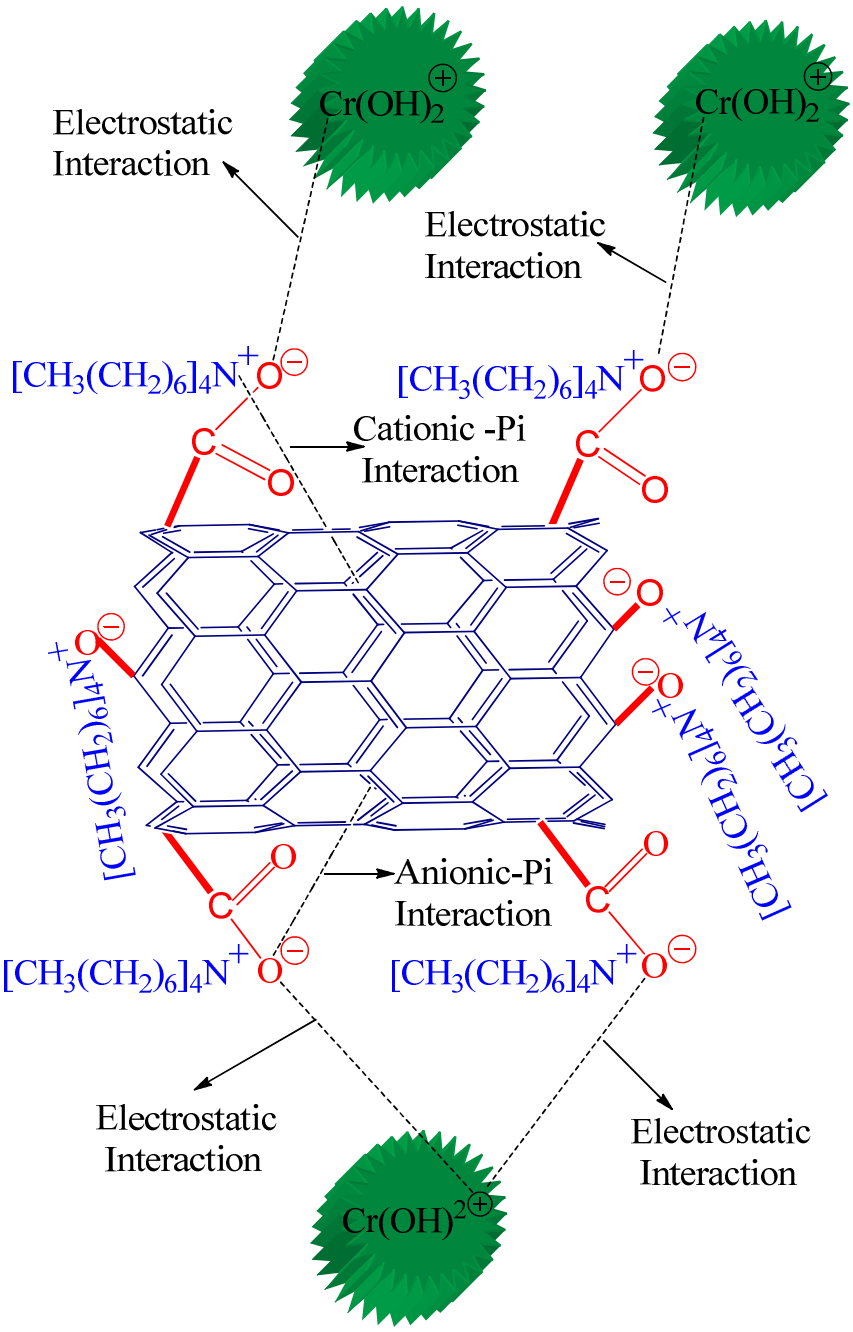

Fig. 11C. Illustration of interaction between IL-oxi-MWCNT's and Cr(III).

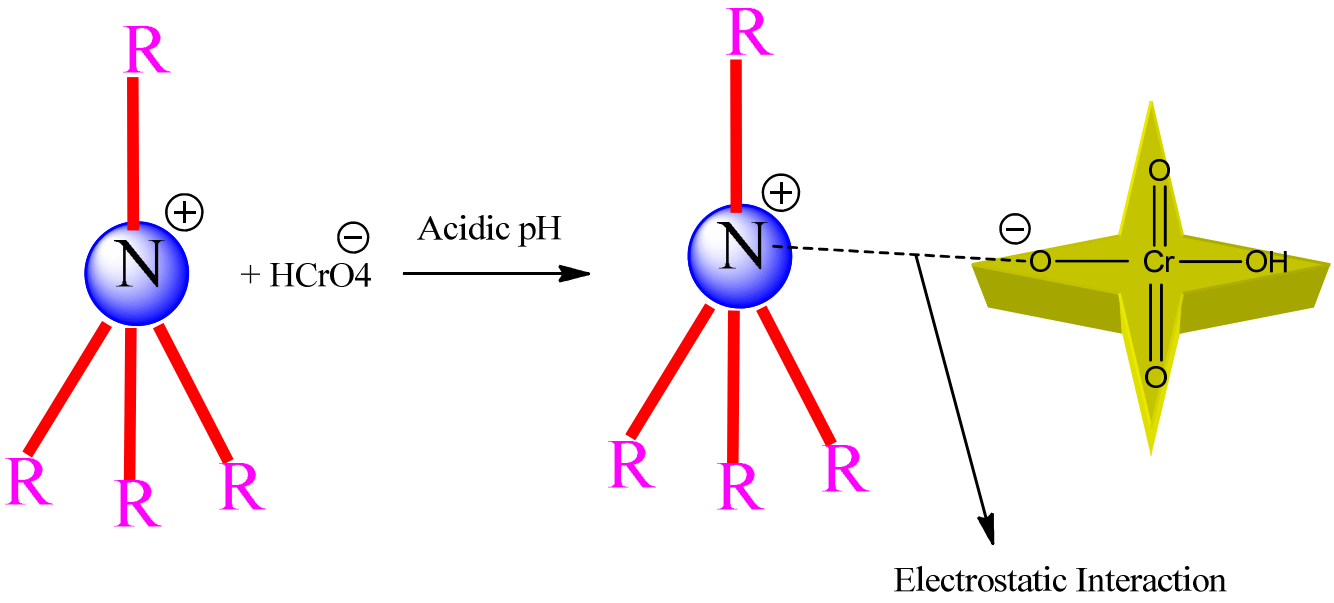

Fig.12A. Conceptual illustration portraying the interaction of Ionic liquid and Cr(VI).

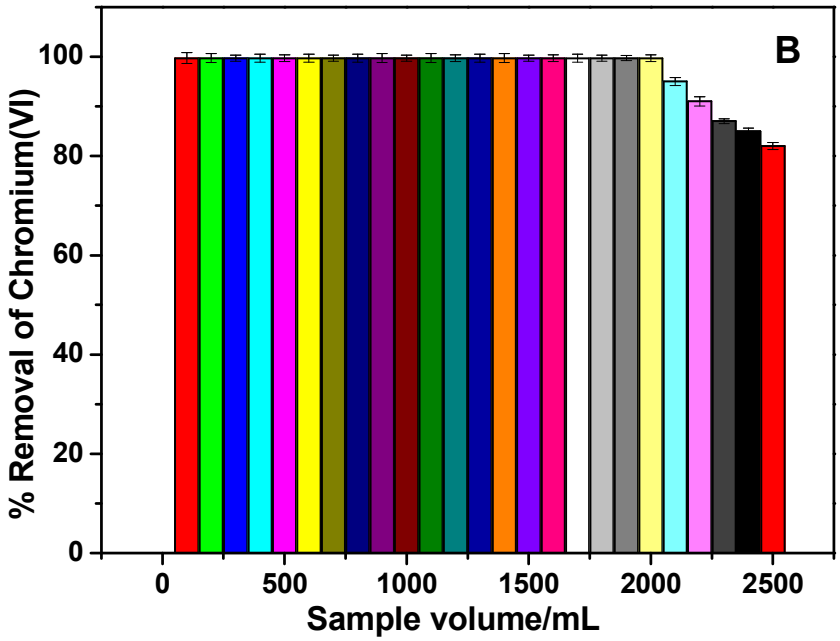

Fig. 12B. Effect of sample volume studies

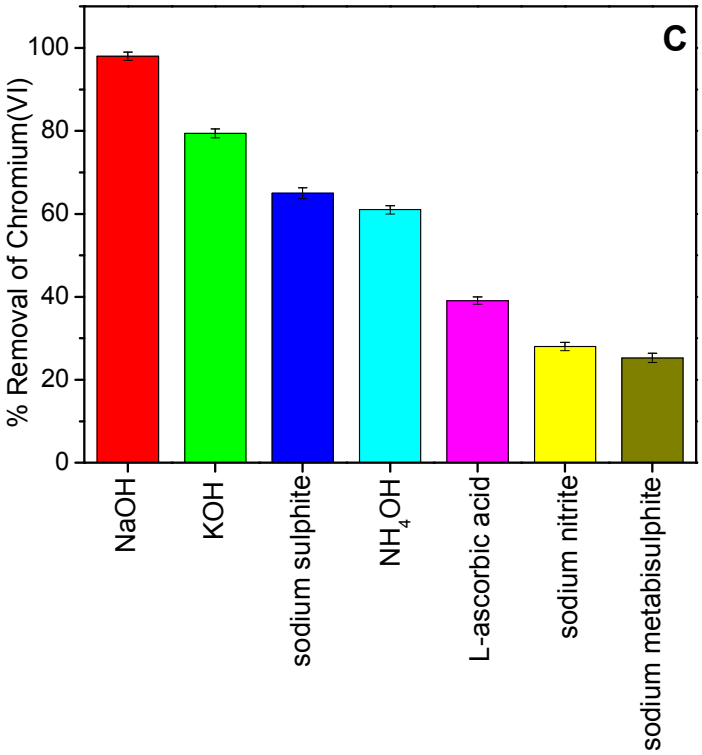

Fig. 12C. Adsorbent regeneration studies

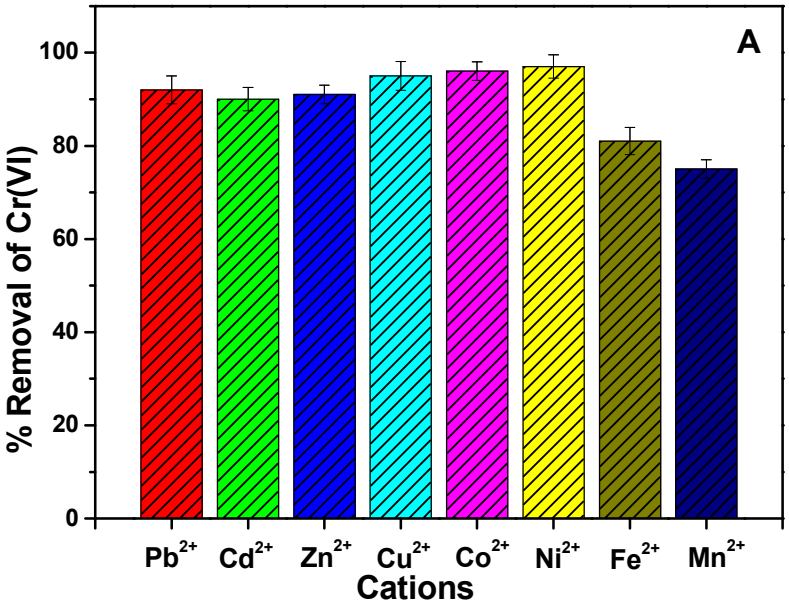

Fig. 13A. Effect of cations.

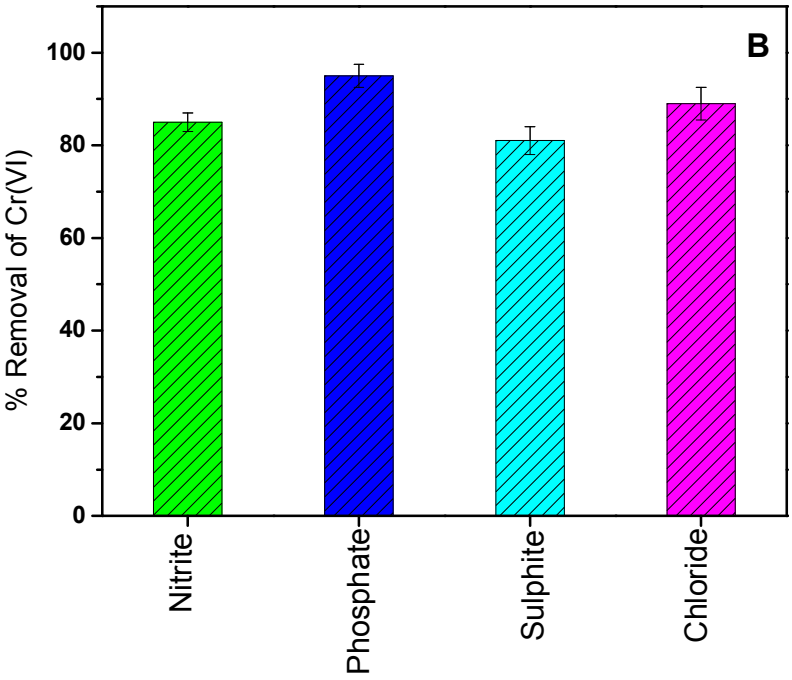

Fig. 13B. Effect of anions.

Table 1. Comparison of adsorption capacity with similar adsorbents

Sl.No	Adsorbent	Adsorption capacity ($mg\ g^{-1}$)	References
1	Ionic liquid impregnated exfoliated graphene oxide	285.71	32
2	Activated carbon supported CNT's	9.0	43
3	Oxidized MWCNT's	2.69	49
4	Smart magnetic graphene	4.86	68
5	CTAB modified graphene	21.57	69
6	Porous Fe_3O_4 hollow microspheres/graphene oxide composite	32.33	70
7	SWCNTs	20.3	71
8	Unmodified MWCNT's	13.2	Present work
9	IL -Functionalized oxi-MWCNT's	85.83	Present work

Table of contents entry:

We report an interesting interaction between multiwalled carbon nanotube (MWCNT's), Tetra n heptylammonium bromide (Ionic Liquid) and Cr(VI)/Cr(III).